Carbohydrate Polymers 91 (2013) 58–67

Contents lists available at SciVerse ScienceDirect

Carbohydrate Polymers

journal homepage: www.elsevier.com/locate/carbpol

Trimethyl and carboxymethyl chitosan carriers for bio-active polymer–inorganic nanocomposites

Georg Geisberger[a], Emina Besic Gyenge[b], Caroline Maake[b], Greta R. Patzke[a,*]

[a] Institute of Inorganic Chemistry, University of Zurich, Winterthurerstrasse 190, CH-8057 Zurich, Switzerland
[b] Institute of Anatomy, University of Zurich, Winterthurerstrasse 190, CH-8057 Zurich, Switzerland

ARTICLE INFO

Article history:
Received 15 May 2012
Received in revised form 17 July 2012
Accepted 4 August 2012
Available online 10 August 2012

Keywords:
Drug carriers
Nanocomposites
Trimethyl chitosan
Polyoxometalates
Anticancer drugs

ABSTRACT

The carrier properties of carboxymethyl chitosan (CMC) and trimethyl chitosan (TMC) in combination with polyoxometalates (POMs) as inorganic drug prototypes are compared with respect to the influence of polymer matrix charge and structure on the emerging composites. A direct crosslinking approach with TMC and $K_6H_2[CoW_{11}TiO_{40}]\cdot 13H_2O$ ($\{CoW_{11}TiO_{40}\}$) as a representative anticancer POM affords nanocomposites with a size range of 50–90 nm. The obtained POM–chitosan composites are characterized with a wide range of analytical methods, and POM encapsulation into positively charged TMC brings forward different nanocomposite morphologies and properties than CMC as a carrier material. Furthermore, uptake of fluorescein isothiocyanate (FITC) labeled POM–CMC and POM–TMC by HeLa cells was monitored, and the influence of chlorpromazine (CP) as inhibitor of the clathrin mediated pathway revealed different cellular uptake behavior of composites and pristine carriers. TMC/$\{CoW_{11}TiO_{40}\}$ nanocomposites are taken up by HeLa cells after short incubation times around 30 min at low concentrations. The anticancer activity of pristine $\{CoW_{11}TiO_{40}\}$ and its TMC-nanocomposites was investigated *in vitro* with MTT assays and compared to a reference POM.

1. Introduction

Drug delivery techniques with abundant, biodegradable and biocompatible polymers are important for efficient therapeutic approaches. Among these carrier matrices, chitosan can be widely functionalized (Andrade et al., 2011; Sonia & Sharma, 2011) for optimal polymer–drug interactions and release properties (Gaspar, Sousa, Queiroz, & Correia, 2011; Janes, Fresneau, Marazuela, Fabra, & Alonso, 2001; Pahwa et al., 2012; van der Lubben, Verhoef, Borchard, & Junginger, 2001). Controlled release of the encapsulated drugs from chitosan derivatives is facilitated through their degradation by ubiquitous enzymes, e.g. chitosanase and lysozyme (Khor, 2001; Nam et al., 2009; Peng, Tseng, Ho, Wei, Liao, & Sung, 2011). Tailored chitosan derivatives open up the way to safe delivery of new drug prototypes, such as the flexible and growing family of transition metal oxide clusters (preferably of W, Mo and V) (Borras-Almenar, Coronado, Müller, & Pope, 2004; Hill, 1998; Miras et al., 2010) known as polyoxometalates (POMs). Over the past decades, the antiviral, antibacterial and anticancer properties of POMs have been extensively reported on (Fluetsch, Schroeder, Gruetter, & Patzke, 2011; Hasenknopf, 2005; Judd et al., 2001; Menon et al., 2011; Pope & Mueller, 1994; Rhule, Hill, & Judd, 1998; Shigeta, Mori, Yamase, Yamamoto, & Yamamoto, 2006). In sharp contrast to their high bio-medical potential that resulted, for example, in a first round of clinical tests against HIV (Moskovitz, 1988), the biochemical pathways (Hungerford, Suhling, & Green, 2008; Ni et al., 1996; Prudent et al., 2008; Zhang et al., 2007) of POMs remain widely unexplored, because their direct monitoring in cells is a considerable challenge. As manifold phenomenological studies on bio-active POMs and composites thereof (Menon et al., 2011) continue to appear (Fluetsch, Schroeder, Gruetter, & Patzke, 2011; Hasenknopf, 2005; Judd et al., 2001; Menon et al., 2011; Pope & Mueller, 1994; Rhule, Hill, & Judd, 1998; Shigeta et al., 2006), while the according pharmaceutical applications still remain to be developed, fundamental studies into the metabolic behavior of POMs are now required. Additionally, the potential adverse effects of POMs, such as cytotoxicity, need to be reduced for their further exploration as interesting candidates for tuneable and low-cost drugs, e.g. through encapsulation techniques (Han et al., 2011; Meissner et al., 2006). Recently, we have established a new chitosan-based drug carrier approach for POMs that addresses the issues of both POM cytotoxicity and cellular tracking in a dual manner (Geisberger, Paulus, Carraro, Bonchio, & Patzke, 2011). POM nanocomposites with carboxymethyl chitosan (CMC) (Chen & Park, 2003; Jeong et al., 2010; Shi, Du, Yang, Zhang, & Sun, 2006) were formed via a gelation approach and have been proven non-cytotoxic. Moreover, their fluorescent labeling permitted the first precise localization of intact POM composites within HeLa cells,

* Corresponding author. Tel.: +41 44 635 4691; fax: +41 44 635 6802.
E-mail address: greta.patzke@aci.uzh.ch (G.R. Patzke).

0144-8617/$ – see front matter © 2012 Elsevier Ltd. All rights reserved.
http://dx.doi.org/10.1016/j.carbpol.2012.08.009

where they quickly assemble in the perinuclear region (Geisberger, Paulus, Gyenge, Maake, & Patzke, 2011). As POMs have been identified as potent enhancing agents for antiviral (Shigeta et al., 1997) and antibacterial drugs (Inoue et al., 2006), the growing family of chitosan derivatives offer new opportunities for targeted delivery strategies.

In this study, we introduce a new nanocomposite type of POMs with trimethyl chitosan (TMC) (Mourya & Inamdar, 2009). The positive charge of TMC is favorable for high solubility at neutral and slightly basic pH values and furthermore permits a direct electrostatic encapsulation of highly negatively charged POM polyanions. This is an advantage over the negatively charged CMC polymer matrix which requires an additional $CaCl_2$-mediated gelation step to incorporate POMs. Given that the surface charge of nanoparticles exerts a tremendous effect on their uptake properties (Huang, Fong, Khor, & Lim, 2005; Mailaender & Landfester, 2009; Verma & Stellacci, 2010) and that positively nanoparticular drug carriers frequently display superior uptake properties (Harush-Frenkel, Debotton, Benita, & Altschuler, 2007) we here explore the multiple functions of TMC as a stabilizer, shuttle and charge compensating carrier for POMs.

TMC keeps attracting considerable research interest for a wide spectrum of drug delivery applications encompassing vaccines, various drugs, e.g. insulin (Mi et al., 2008) or desmopressin (Polnok, Verhoef, Borchard, Sarisuta, & Junginger, 2004), small molecules and DNA (Mourya & Inamdar, 2009). TMC is suitable for opening tight junctions (van der Merwe, Verhoef, Verheijden, Kotzé, & Junginger, 2004) and thus facilitates drug delivery in physiological media (Mourya & Inamdar, 2009) or brain drug delivery with low toxicity (Wang et al., 2010). Additionally, TMC opens up manifold chemical routes toward N-alkyl and N-aryl TMCs with individual bio-active profiles, such as antibacterial activity (Jia, Shen, & Xu, 2001). Currently, such compounds are further subjected to grafting processes with other polymers (e.g. PEG) (Liang, Sun, Duan, & Cheng, 2012), thereby paving the way to a new arsenal of copolymeric drug delivery vehicles, and TMC-based crosslinked polymers are used in various nasal vaccination strategies (Slütter & Jiskoot, 2010). The internalization pathways of chitosan-based nanoscale drug carriers often follow diverse endocytosis mechanisms (Park et al., 2010). As a consequence, non-toxic TMC-based polymer shuttles are interesting candidates for the controlled delivery of POMs in order to obtain the long sought-after insight into their behavior under physiological conditions that is still missing for their pharmacological evaluation. Vice versa, POMs serve as model compounds for the interaction of TMC matrices with negatively charged guest molecules.

Inspired by reports on successful anticancer drug delivery with TMC (Liu et al., 2010) and its promising biocompatibility and antitumoral carrier properties *in vivo* (Guan et al., 2012), we studied TMC nanocomposites with $K_6H_2[CoW_{11}TiO_{40}]\cdot 13H_2O$ (henceforth abbreviated as $\{CoW_{11}TiO_{40}\}$) as a representative POM with proven biological and antitumoral activity (Mueller et al., 2006; Wang, Liu, & Pope, 2003; Yang, He, Wang, Li, & Liu, 2004). $\{CoW_{11}TiO_{40}\}$ is furthermore suitable for anticancer composite formation with liposome (Wang, Li, Liu, & Pope, 2005; Yang et al., 2004) and starch (Wang et al., 2003; Zhai, Li, Zhang, Wang, & Li, 2008) as carriers. In the following, we compare the influence of CMC and TMC polymer matrices on the particle size, morphology and surface charge of the resulting hybrid nanocomposites. The influence of the different polymer charges on the uptake efficiency and mechanisms of their respective POM composites is investigated. Furthermore, cellular uptake of FITC-labeled $\{CoW_{11}TiO_{40}\}$–TMC nanocomposites is monitored and the anticancer activity of the new nanomaterials is compared to reference POM–TMC composites.

2. Experimental

2.1. Materials

Chitosan (LMW, 20 kDa, degree of deacetylation > 85%) was purchased from Sigma–Aldrich. All other used reagents were purchased from Sigma–Aldrich or Acros as ACS reagents and used as received.

2.2. Synthesis of POMs

$K_7H[Nb_6O_{19}]$, α_2-$K_{10}[P_2W_{17}O_{61}]\cdot 20H_2O$ and $K_{14}[Na(H_2O)P_5W_{30}O_{110}]\cdot 31H_2O$ were synthesized according to refs. (Alizadeh, Harmalker, Jeannin, Martinfrere, & Pope, 1985; Dickman, Gama, Kim, & Pope, 1996; Edlund, Saxton, Lyon, & Finke, 1988; Ginsberg, 1990).

α_2-$K_7[P_2W_{17}(NbO_2)O_{61}]\cdot 13H_2O$ (Judd et al., 2001): $K_7H[Nb_6O_{19}]$ (55 mg, 0.475 mmol) was dissolved in an aqueous H_2O_2 solution (7.00 mL, 1.5%). HCl (0.20 mL, 4 M) and α_2-$K_{10}[P_2W_{17}O_{61}]\cdot 20H_2O$ (0.66 g, 0.145 mmol) in H_2O_2 (20 mL, 1.5%) were added. HCl (4 M) was added to adjust the pH to 1.1 and KCl (1.0 g, 12.4 mmol) was added. The volume of the solution was reduced in a stream of nitrogen for 12 h. Yellow crystals were formed after the solution was stored for 24 h at 4 °C. The crystals were collected by filtration. Yield: 80 mg (13%).

$K_6H_2[CoW_{11}TiO_{40}]\cdot 13H_2O$ (Chen and Liu, 1997): $Na_2WO_4\cdot 2H_2O$ (1.8256 g, 5.5 mmol) was dissolved in water (10 mL). The pH was adjusted to 6.31 with glacial acetic acid and a solution of $Co(CH_3COO)_2\cdot 4\,H_2O$ (0.1228 g, 0.52 mmol) in water (1 mL) was added dropwise. Afterwards, $TiOSO_4$ (0.16 g, 1.0 mmol) dissolved in 0.1 M H_2SO_4 (1 mL) was added dropwise. The mixture was heated to reflux for 1 h and was then allowed to cool to room temperature. KCl (0.6 g) was added in small portions until no further precipitation was observed. The precipitate was collected by filtration and recrystallized twice from hot water. The product was obtained as blue crystals. Yield: 0.25 g (15%).

2.3. Synthesis and FITC labeling of carboxymethyl chitosan (CMC)

CMC with a degree of substitution of 1.4 per sugar unit and a molecular weight of 20 kDa was prepared as described in ref. (Geisberger, Paulus, Carraro, et al., 2011).

CMC: NaOH (6.75 g) was dissolved in a mixture of deionized water and isopropanol (1:4, 50 mL). Chitosan (5 g) was added and alkalized in this mixture at 50 °C for 1 h. Monochloroacetic acid (7.5 g) was dissolved in isopropanol (10 mL) and slowly added to the reaction mixture over 30 min at 50 °C. The reaction was quenched after 4 h of stirring at 50 °C by addition of ethanol (70%, 100 mL) to the reaction mixture. After collection by filtration the product was extensively washed with 70–94% ethanol to remove residual amounts of salt and water, dialyzed for two days against distilled water and dried by lyophilization. Yield: 10.75 g, white solid.

FITC–CMC: CMC (30 mg) was dissolved in 3 mL distilled H_2O, and a solution of FITC (3 mg) in dry MeOH (4.5 mL) was added, yielding a fluorescent orange mixture which was stirred for 4 h in the dark at room temperature. Afterwards, the solvent was reduced to 1 mL under vacuum and an orange solid precipitated upon addition of ethanol. The solid was washed thoroughly with ethanol until the washing solution showed no more fluorescence. The product was dried under high vacuum and stored in the dark at 4 °C.

2.4. Synthesis and FITC labeling of trimethyl chitosan (TMC)

O-methylated trimethyl chitosan with a degree of quaternization of 20% and a molecular weight of 20 kDa was prepared as described in ref. (Verheul et al., 2008). Chitosan (0.50 g) and sodium

iodide (1.20 g) were suspended in NMP (20 mL). A NaOH solution (3 mL, 15% v/w) was added and the mixture was heated to 60 °C for 20 min. Subsequently, methyl iodide (3 mL) was added and the reaction mixture was heated to 60 °C for 60 min. The reaction was quenched by pouring the reaction mixture into a mixture of diethyl ether and ethanol (100 mL, 1:1). The obtained precipitate was collected by filtration and washed with diethyl ether. Ion exchange was performed by dissolving the precipitate in water (50 mL) and a subsequent dialysis against a 1% NaCl solution for two days. Afterwards, the solution was dialyzed against distilled water for two days. The pure product was obtained by lyophilization.

FITC–TMC: TMC (30 mg) was dissolved in 3 mL distilled H_2O, and a solution of FITC (3 mg) in dry MeOH (4.5 mL) was added, yielding a fluorescent orange mixture which was stirred for 4 h in the dark at room temperature. Afterwards, the solvent was reduced to 1 mL under vacuum and an orange solid precipitated upon addition of ethanol. The solid was washed thoroughly with ethanol until the washing solution showed no more fluorescence. The product was dried under high vacuum and stored in the dark at 4 °C.

2.5. Synthesis of POM–CMC nanoparticles

A typical synthesis of POM–CMC nanoparticles proceeds as follows: low molecular weight CMC (2 mg) was dissolved in distilled H_2O (4 mL). The pH was adjusted to 7 with HCl (0.02 M) and the respective POM (0.4–2 μmol) was added. Stirring was continued for at least 30 min to distribute the POM homogeneously in solution. Afterwards, an aqueous $CaCl_2$ solution (2 mg/mL, 0.5 mL) was added dropwise over 3 min. The solution turned opalescent as an indication of nanoparticle formation.

2.6. Synthesis of POM–TMC nanoparticles

A solution of the respective POM (0.01–0.6 μmol) was added dropwise to a solution of TMC in 1 mL distilled water (0.25–1.0 mg/mL) until the desired TMC/POM ratio was reached. The dropwise addition of the POM solution has to be carried out very carefully over at least 10 min depending on the amount of POM solution added. During the whole time the TMC solution has to be stirred vigorously or sonicated. The formation of nanoparticles is indicated by a slight opalescence of the solution. For all DLS measurements a TMC to POM ratio of 1:0.05 was applied.

2.7. Cultivation of HeLa cells

HeLa cells were cultivated in Dulbecco's Modified Eagle Medium (DMEM, Sigma–Aldrich) containing 4500 mg/L glucose, 5 mM L-glutamine, 1 mM sodium pyruvate and 1 mM sodium bicarbonate, supplemented with 10% heat inactivated FCS (Fetal Calf Serum, Sigma–Aldrich) in a humidified atmosphere at 37 °C and 5% CO_2. The passage of the adherent monolayer cells was performed after the cells reached a confluence of approximately 80% by trypsinization with 0.1% trypsin-EDTA (0.05% trypsin and 0.02% EDTA in PBS, pH 7.3, Sigma–Aldrich).

2.8. Cellular uptake tests

HeLa cells were seeded onto 96-well plates (Corning) at a density of 3000 cells per well in DMEM and incubated over night under standard conditions (37 °C, 5 % CO_2, humidified atmosphere). The medium was replaced by different DMEM solutions containing the nanocomposites in various concentrations (6.25, 12.5, 25 μg/mL, TMC/POM ratio = 1:0.1, CMC/POM ratio = 5:0.1) and the cells were incubated in these solutions for 15 min and 1, 3, 7, 24 h. Afterwards, the solutions were removed and the cells were washed five times with PBS to remove particles which were not located inside the cells. The fluorescence was recorded at 530 nm using a microplate luminometer (synergy2, BioTek). Solutions of FITC–TMC and FITC–CMC with equal concentrations were used as references. For inhibition tests HeLa cells were pre-incubated with chlorpromazine (10 μg/mL) for 60 min. Sextets were performed for each concentration and incubation time to determine the standard deviation.

2.9. MTT assay

HeLa cells were seeded onto 96-well plates (Corning) at a density of 3000 cells per well in DMEM and incubated over night under standard conditions (37 °C, 5 % CO_2, humidified atmosphere). The medium was replaced by different DMEM solutions containing either TMC, nanocomposites or POMs in different concentrations (12.5, 25, 50 μg/mL, TMC/POM ratio = 1:0.1) and the cells were incubated in these solutions for 1, 2, 5 and 24 h. After removing the solutions, DMEM containing MTT (0.5 mg/mL) was added to the cells. During an additional incubation time of 3 h MTT is converted by the living cells. The metabolic product formazan was solubilized by replacing the MTT containing medium against dimethyl sulfoxide. After mixing, the optical density was recorded at 565 nm using a microplate luminometer (synergy2, BioTek). For each concentration and incubation time sextets were performed to determine the standard deviation. Results are expressed as means ± SD. Data was analyzed by one-way ANOVA with the *post hoc* Tukey's test applied for paired comparisons ($p < 0.05$; Prism3).

2.10. Stability tests

Two solutions were prepared, containing either $\{CoW_{11}TiO_{40}\}$ (100 μg/mL) or TMC/$\{CoW_{11}TiO_{40}\}$ composites (TMC/POM ratio = 1:0.1, $\{CoW_{11}TiO_{40}\}$ content 100 μg/mL), respectively. UV/vis spectra (225–325 nm) for both solutions were recorded daily at the same time over a period of 4 d. The characteristic W—O—W absorption band around 260 nm was used to demonstrate the degradation of the pristine POMs versus the nanocomposites.

2.11. Encapsulation

For the measurement of the encapsulation efficiency the absorptions of three nanoparticle solutions with different TMC to POM ratios (1:0.5, 1:0.2, 1:0.1) were recorded on a PerkinElmer Lambda 650S UV/Vis spectrometer. Afterwards, the solutions were centrifuged at 13,200 rpm and a temperature of 4 °C for 30 min. The pellets were removed and the absorption of the supernatant liquid after centrifugation was recorded. Encapsulation efficiency was calculated from absorption differences before and after centrifugation, based on the absorption value at 625 nm.

2.12. Release study

TMC/$\{CoW_{11}TiO_{40}\}$ composites were prepared as described above and the release study was performed as described in (Zhang & Neau, 2001). For the *in vitro* release of $\{CoW_{11}TiO_{40}\}$, 5 mL of a 0.1 M acetate buffer solution containing the nanocomposites (1 mg/mL, pH 6, TMC/POM ratio = 1:0.1) and β-glucosidase (0.05% w/v) were introduced into a dialysis tube (Snakeskin, MWCO 3500) which was placed in 20 mL of 0.1 M acetate buffer release media. The media was stirred at 37 °C and at predetermined time intervals (1, 2, 3, 4, 5, 6, 7, 8, 9, 24, 48 h) aliquots were collected from the media outside the dialysis tube and the amount of cobalt was determined with a Varian AA240FS atomic absorption spectrometer equipped with a graphite furnace.

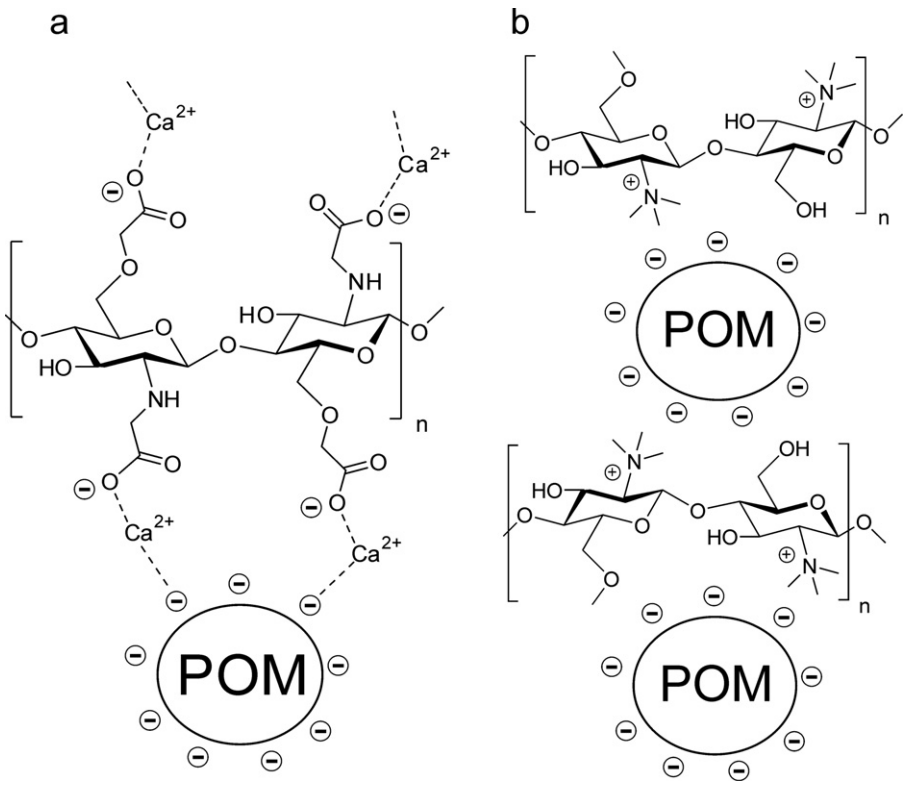

Fig. 1. Electrostatic interaction of CMC (a) and TMC (b) biopolymer matrices with encapsulated POMs.

2.13. Analytical characterization of nanocomposites

Fourier transform infrared (FT-IR) spectra were recorded on a Perkin-Elmer BXII spectrometer with KBr pellets. Analytical samples were prepared by centrifugation of the nanoparticle solution at 13,200 rpm for 30 min at a temperature of 4 °C. To remove an excess of POMs, several centrifugation runs were performed, followed by lyophilization.

UV/vis spectra were recorded on a PerkinElmer Lambda 650S UV/Vis spectrometer with a 10 mm cuvette. Particle size and zeta potential were measured with dynamic light scattering on a Zetasizer Nano ZS90 (ZEN3690, Malvern Instruments) using a quartz cuvette containing 1 mL of the solution under investigation. For zeta potential measurements the quartz cuvette was additionally equipped with a Universal Dip cell (ZEN1002, Malvern Instruments). TEM measurements were performed using the negative contrast method. 300 mesh copper grids were rendered hydrophilic by glow discharge, followed by immediate treatment with the nanoparticle solution for 1 min. The solution was removed and TEM investigations were performed on a FEI Tecnai G2 Spirit transmission electron microscope (120 kV, LaB_6).

3. Results and discussion

3.1. Formation of POM–TMC nanocomposites

POM–TMC nanoparticles are obtained from the direct electrostatic interaction of positively charged TMC with negatively charged POMs (Fig. 1), whereas POM–CMC composite formation proceeds via a $CaCl_2$-mediated gelation approach (cf. Section 2) (Geisberger, Paulus, Carraro, et al., 2011). The TMC crosslinking process is more straightforward: POM solutions are slowly dropped into a stirred or sonicated (Delmas et al., 2011) TMC solution to distribute the POMs evenly and to prevent particle aggregation. The particle size of the POM–TMC composites can furthermore be addressed *via* the preparative parameters, especially the rate of POM addition, stirring and sonication. As expected, POM–TMC composites formed under the influence of sonication generally exhibit smaller particle sizes and more homogeneous particle size distributions in comparison with products obtained from stirred reaction mixtures.

3.2. Particle size and zeta potential determinations

Particles sizes of POM–CMC and POM–TMC nanocomposites were measured with dynamic light scattering (DLS). The combination of CMC with POMs displays a trend toward larger particles sizes than POM–TMC (Table 1). This may be due to the different crosslinking strategy employed for the synthesis of POM–TMCs. The more direct electrostatic interactions between POM and TMC in comparison with CMC (cf. Fig. 1) might give rise to a different nucleation process during composite formation. The zeta potential of the POM–TMC and POM–CMC nanocomposites strongly depends on the biopolymer matrix. The presence of carboxylic groups in CMC shifts the zeta potential of the composites to negative values of −17.3 and −18.7 mV, respectively. Likewise, the positively charged trimethylamino functionalities of TMC lead to positive zeta potential values of 55.4 and 61.6 mV (Table 1). Figs. S1 and S2 show representative size distributions and zeta potential measurements.

Table 1
Particle sizes with polydispersity indices (PdI) and zeta potentials with standard deviation of POM–CMC and POM–TMC composites.

	POM–CMC	POM–TMC
Particle size/nm (PdI)		
$\{CoW_{11}TiO_{40}\}$	131.3 (0.127)	61.1 (0.102)
$\{NbO_2P_2W_{17}O_{61}\}$	173.3 (0.141)	80.7 (0.177)
Zeta potential/mV (deviation/mV)		
$\{CoW_{11}TiO_{40}\}$	−17.3 (5.78)	55.4 (6.16)
$\{NbO_2P_2W_{17}O_{61}\}$	−18.7 (4.11)	61.6 (5.01)

Table 2
Particle size and polydispersity indices (PdI) for different initial TMC/POM ratios.

POM (μmol)	TMC/POM ratio (mg)/(μmol)	Particle size (nm)	PdI
0.02	1:0.02	78.1	0.294
0.05	1:0.05	54.8	0.224
0.1	1:0.1	61.9	0.131
0.15	1:0.15	55.1	0.094
0.2	1:0.2	61.1	0.102
0.3	1:0.3	63.7	0.094
0.4	1:0.4	114.0	0.090
0.5	1:0.5	85.3	0.055
0.6	1:0.6	84.4	0.090

3.3. Particle size trends

The average particle size range of POM–TMC nanocomposites investigated in the present study ($\{CoW_{11}TiO_{40}\}$ and $K_7[P_2W_{17}(NbO_2)O_{61}]\cdot 13H_2O$ ($\{NbO_2P_2W_{17}O_{61}\}$) as a reference) was determined as 50–90 nm with DLS measurements. Detailed parameter studies were performed with $\{CoW_{11}TiO_{40}\}$ as a bio-active POM (cf. sections below) over a range of TMC/POM ratios between 1:0.02 and 1:0.6 (Table 2). No clear trend among the particle sizes could be observed for TMC/POM ratios up to 1:0.3 while higher POM contents led to increased particle sizes. POM–TMC composites obtained from an initial 1:0.3 ratio were stable in solution over several days up to several weeks without any aggregation effects. The amount of encapsulated POMs within the TMC matrix is ca. 6-fold higher than the POM:CMC ratios observed in the course of our previous studies (Geisberger, Paulus, Carraro, et al., 2011). This is probably resulting from the facile and direct electrostatic POM–TMC interaction (Fig. 1).

As the stability of bio-active POMs under physiological conditions is relevant for their application potential, we have performed according tests on selected target POMs of the present study. $\{CoW_{11}TiO_{40}\}$ has been classified as stable in the pH range 4.7–6.7 (Wang et al., 2003), and preceding UV/vis studies at pH 7.4 reported stability for min. 50% of a $\{CoW_{11}TiO_{40}\}$ sample after 24 h (Mueller et al., 2006). We have thus compared the UV/vis spectra of $\{CoW_{11}TiO_{40}\}$ and TMC/$\{CoW_{11}TiO_{40}\}$ over a period of 4 d at pH 7.4 (Fig. 2). Whereas the pristine POM undergoes a shift of the characteristic W—O—W absorption band around 260 nm, the composite displays only minor changes of the absorption characteristics over the entire period, thus indicating a high degree of POM stability after encapsulation. Given that composite formation of negatively charged POMs with the positively charged TMC matrix (Fig. 1b) is a very rapid process, the TMC matrix is capable of trapping intact $\{CoW_{11}TiO_{40}\}$ to form stable composites (Figs. 2 and 3). Additional ^{31}P NMR investigations on a representative phosphorus

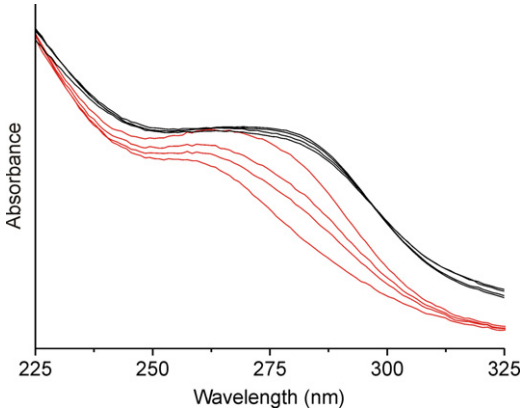

Fig. 2. UV/vis stability tests (PBS buffer, pH 7.4) of $\{CoW_{11}TiO_{40}\}$ (red) and TMC/$\{CoW_{11}TiO_{40}\}$ (black) over 4 d (top to bottom line: 1 d–4 d).

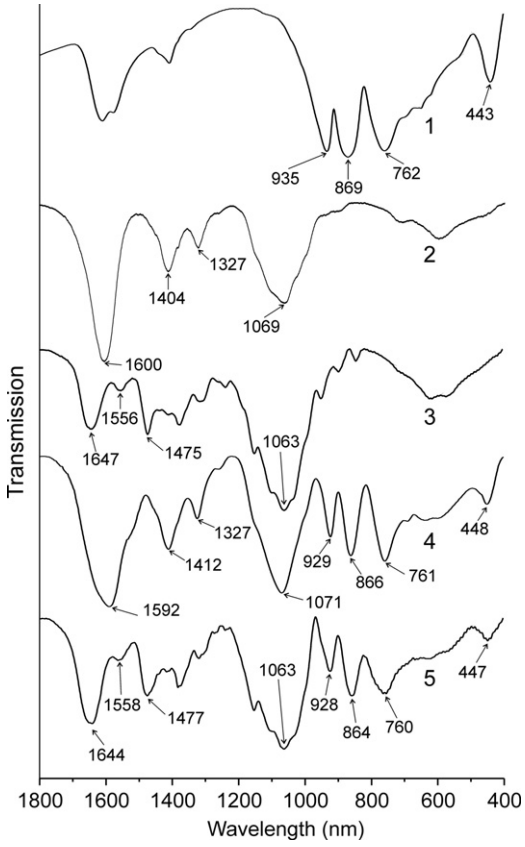

Fig. 3. FT-IR spectra of (1) $\{CoW_{11}TiO_{40}\}$, (2) CMC, (3) TMC, (4) CMC/$\{CoW_{11}TiO_{40}\}$, (5) TMC/$\{CoW_{11}TiO_{40}\}$; CMC:POM and TMC:POM ratio = 2:0.1.

containing POM ($K_{14}[Na(H_2O)P_5W_{30}O_{110}]\cdot 31H_2O$) show no significant differences between pristine and encapsulated POM, thus providing further evidence for the incorporation of intact POMs by TMC and CMC (Fig. S3).

3.4. Spectroscopic and electron microscopy comparison of POM–CMC and POM–TMC composite formation

The encapsulation of $\{CoW_{11}TiO_{40}\}$ is evident from FT-IR spectra (Fig. 3). The characteristic peaks in the IR spectrum of $\{CoW_{11}TiO_{40}\}$ at 443, 762, 869, and 935 cm^{-1} can be clearly assigned to (Co—O2), (W—O1—W), (W—O4—W), and (W=O3), respectively (Kraus, Stephan, Rollich, Matejka, & Reck, 2005). CMC can be identified through key vibrations at 1069 cm^{-1} (CH—OH stretch), 1327 cm^{-1} (CH_2 wagging), 1404 cm^{-1} (carboxyl group symmetric stretch), and 1600 cm^{-1} (carboxyl group asymmetric stretch) (Mourya, Inamdar, & Tiwari, 2010). The IR spectrum of TMC contains characteristic peaks at 1063 cm^{-1} (CH—OH stretch), 1475 cm^{-1} (C—H of methyl groups, asymmetric angular deformation), 1556 cm^{-1} (NH_2, non-methylated), and 1647 cm^{-1} (quaternary ammonium salt) (Mourya & Inamdar, 2009).

All characteristic absorption bands of the POM as well as of the CMC and TMC matrix materials do not display significant shifts, thereby indicating that the encapsulation process does not affect the structure of the components. According FT-IR spectra for $\{NbO_2P_2W_{17}O_{61}\}$ are shown in Fig. S4.

The encapsulation efficiency for TMC was investigated with UV/vis spectroscopy (characteristic band between 550 and 680 nm), and Fig. 4 shows representative results for different TMC/$\{CoW_{11}TiO_{40}\}$ ratios with increasing POM contents. The degree of POM encapsulation was determined from the difference in absorption intensities at 625 nm before and after centrifugation.

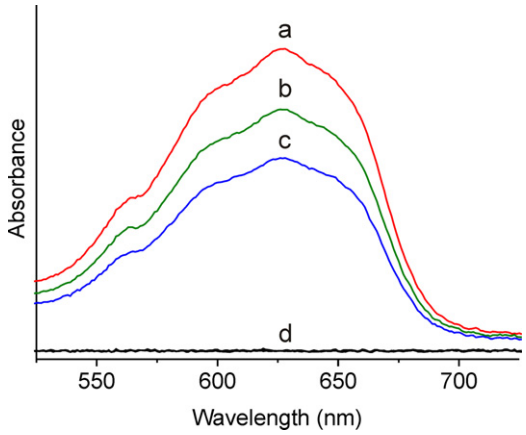

Fig. 4. Representative UV/vis spectra of TMC/{$CoW_{11}TiO_{40}$} formation showing the encapsulation efficiency for different TMC/{$CoW_{11}TiO_{40}$} ratios: (a) 1:0.5, (b) 1:0.2, (c) 1:0.1, (d) absorption after centrifugation.

As the residual POM absorption in the supernatant liquid vanishes entirely after centrifugation of the composites, they are quantitatively encapsulated (ca. 99%) in the biopolymeric matrix, which is in line with our previously reported quantitative uptake of POMs by CMC (Geisberger, Paulus, Carraro, et al., 2011).

Transmission electron microscopy (TEM) investigations were performed to complement DLS measurements with morphology characterizations. Representative results on {$CoW_{11}TiO_{40}$}-based composites are shown in Fig. 5, and the particle sizes determined from TEM micrographs generally agree well with those determined from DLS (Tables 1 and 2). Interestingly, the composite morphology depends strongly on the biopolymer: the majority of the as-synthesized POM–TMC composites are below 100 nm in size and exhibit less regular morphologies than we had observed for spherical POM–CMC composites (Geisberger, Paulus, Carraro, et al., 2011). This also corresponds to previous reports on inhomogeneous morphologies of TMC- and chitosan-based materials (Peng et al., 2011; Wan, Sun, Li, & Li, 2008). Reference experiments concerning the influence of drug carrier type and crosslinker on the particle shape showed that crosslinking of TMC with sodium triphosphate affords homogeneous spherical particles (Fig. S5), while chitosan-based materials with sodium triphosphate and POMs as crosslinkers exhibit inhomogeneous morphologies (Fig. S6).

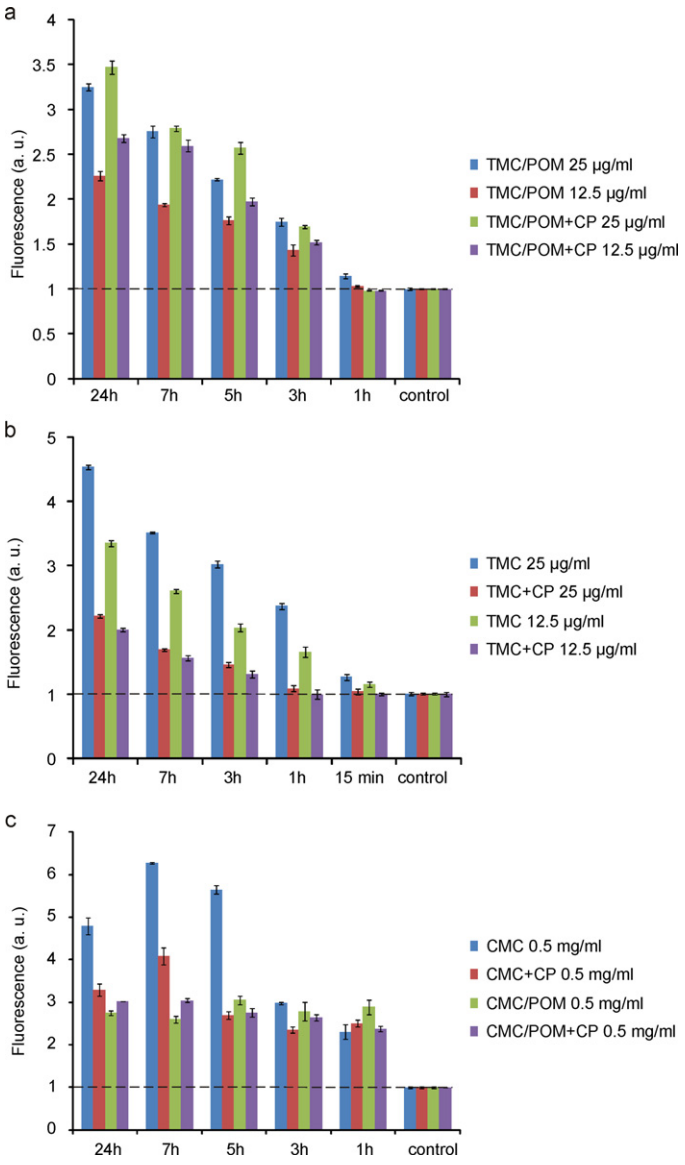

Fig. 6. (a) Uptake of FITC-TMC-POM nanocomposites and (b) pristine FITC-TMC by HeLa cells in the presence and absence of chlorpromazine (CP) at different incubation times and concentrations; (c) uptake of FITC-CMC-POM nanocomposites and pristine FITC-CMC by HeLa cells in the presence and absence of CP at different incubation times (control = pristine HeLa cells in the absence of POMs and biopolymer).

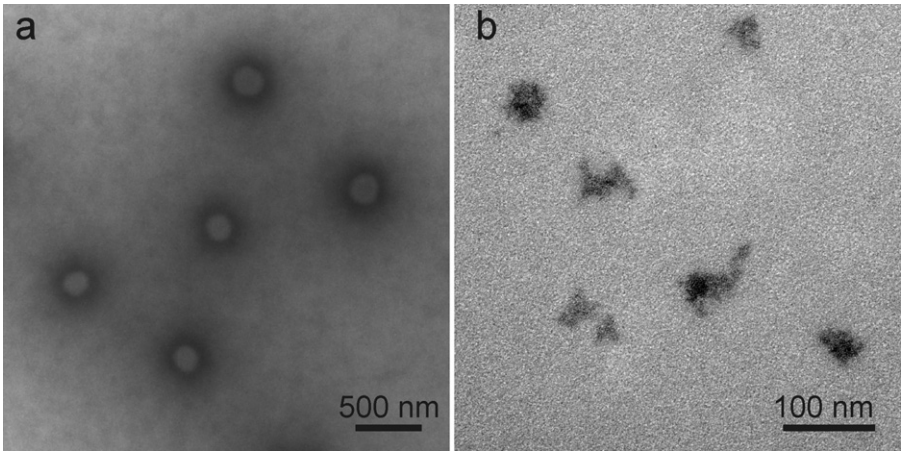

Fig. 5. Representative TEM images of (a) CMC/{$CoW_{11}TiO_{40}$} composites and (b) TMC/{$CoW_{11}TiO_{40}$} composites.

3.5. POM–CMC vs. POM–TMC composites: fluorescence monitoring

Both TMC and CMC were labeled with fluorescein isothiocyanate (FITC) for monitoring of their cellular uptake with confocal laser scanning microscopy. $\{NbO_2P_2W_{17}O_{61}\}$-composites were selected as a reference system with a non-cytotoxic antiviral POM (Judd et al., 2001) and they were incubated with HeLa cells at various concentrations for different incubation times (Fig. 6). Furthermore, selected samples were pre-incubated with chlorpromazine (CP) to investigate the role of clathrin mediated pathways in the overall composite uptake process.

Generally, the incorporation of TMC and its composites by HeLa cells is superior to the CMC analogs which require 10–20 fold higher concentrations to achieve uptake of comparable particle amounts. POM–TMC composites and pristine TMC exhibit a steady uptake behavior up to 24 h, while the uptake of POM–CMC particles as well as of pristine CMC reaches a maximum after 7 h (Fig. 6). Pristine CMC is taken up more readily by the cells than the composites for the first 7 h, followed by decline of the fluorescence signal. Whereas the POM–TMC uptake proceeds continuously, maximum concentrations of POM–CMC nanoparticles are already reached after 1 h. The significant uptake differences between POM–TMC and POM–CMC nanocomposites are due to the above-mentioned differences in particle charge, size and morphology. This is in line with previous studies on the interaction of nanoparticles with cells (Mailaender & Landfester, 2009) which demonstrate a significant dependence of cellular uptake on surface properties and charge of the respective nanoparticles (Huang et al., 2005; Verma & Stellacci, 2010). Negatively charged particles, for example, are often less readily taken up by cells which corresponds with our observation that positively charged POM–TMC composites display better uptake behavior than negatively charged POM–CMC particles (Table 1) (Huang et al., 2005). To the best of our knowledge, no data on the influence of CP on the cellular uptake behavior of CMC, TMC and composites thereof are available to date. Interestingly, the cellular uptake of POM–TMC and POM–CMC composites is not hindered by CP addition (Fig. 6). While POM–CMC uptake remains more or less constant, POM–TMC uptake is significantly enhanced in comparison with CP-free experiments. The inhibition of the clathrin mediated pathway by CP might promote other mechanisms which in turn facilitate POM–TMC nanoparticle uptake. However, the uptake behavior of pristine CMC differs entirely from POM–CMC composites: CMC uptake is partially inhibited by CP, particularly for incubation times > 1 h. Likewise, uptake of pristine TMC is hindered by CP addition, following a comparable timescale. These results indicate that the biopolymeric drug carrier matrices are probably partially incorporated via the clathrin mediated endocytosis pathway, while the POM–composites follow a different metabolic route. Macropinocytosis and caveolae-mediated pathways are probably involved in nanoparticle uptake as indicated by recent studies on FITC-chitosan-based gene delivery vectors (Peng et al., 2011).

3.6. CLSM monitoring of POM–TMC nanocomposites

TMC/$\{CoW_{11}TiO_{40}\}$ nanocomposites were selected as a bioactive model system for uptake investigations with HeLa cancer

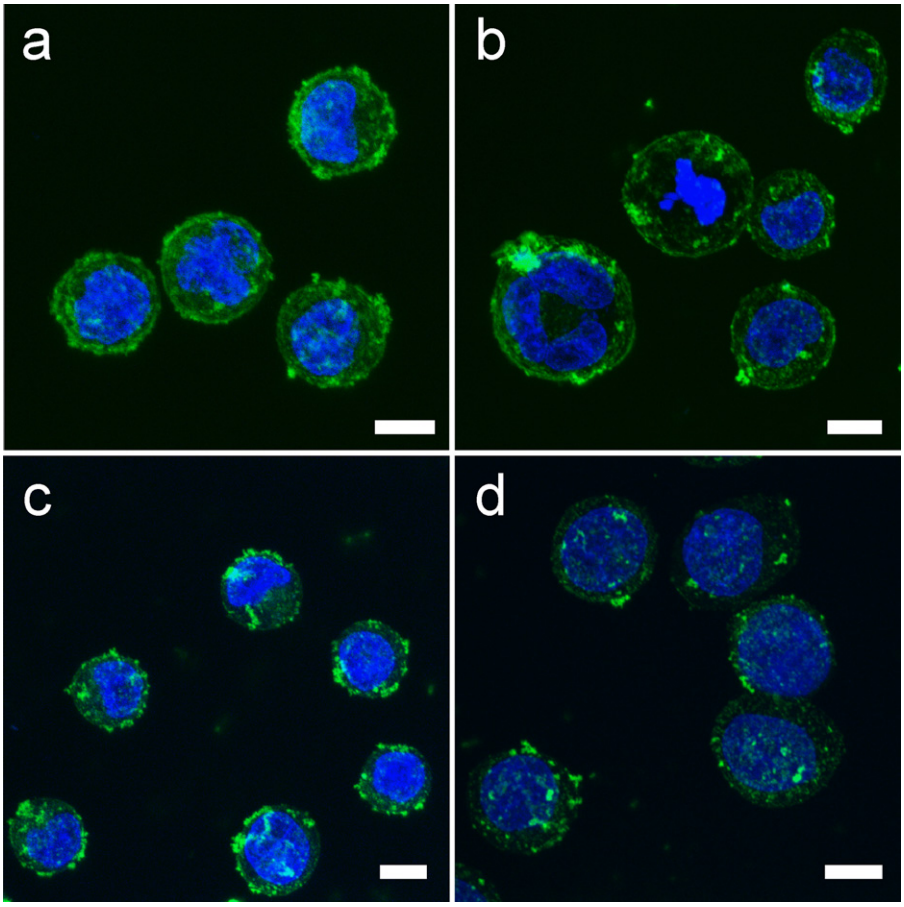

Fig. 7. Uptake of FITC labeled TMC/$\{CoW_{11}TiO_{40}\}$ nanocomposites monitored with confocal laser scanning microscopy for different concentrations after various incubation times (scale bar = 10 μm; nucleus = blue; nanocomposites = green): (a) 25 μg/mL, 2 h; (b) 25 μg/mL, 0.5 h; (c) 12.5 μg/mL, 2 h; (d) 12.5 μg/mL, 0.5 h. (For interpretation of the references to color in this figure legend, the reader is referred to the web version of the article.)

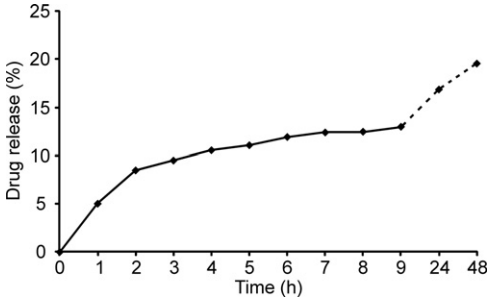

Fig. 8. *In vitro* release profile of $\{CoW_{11}TiO_{40}\}$ from TMC/$\{CoW_{11}TiO_{40}\}$ conjugates (AAS monitoring).

cells using confocal laser scanning microscopy. Fig. 7 shows HeLa cells incubated with TMC/$\{CoW_{11}TiO_{40}\}$ after 30 min and 2 h, respectively. Cellular uptake of a 25 μg/mL nanoparticle solution after 2 h and 30 min is shown in Fig. 7a and b, while Fig. 7c and d illustrate the uptake of a 12.5 μg/mL composite solution after the same incubation times. Cellular uptake of TMC/$\{CoW_{11}TiO_{40}\}$ proceeds rapidly as can be seen from the considerable amounts of particles detected within the cells after 30 min at rather low concentrations, which points to a high uptake efficiency. Interestingly, the cells display rounding and loss of adhesion after 30 min which might indicate the onset of cell death (Zhai et al., 2008).

This affection of HeLa cells was not observed for pristine POM or TMC (Fig. S7) and can thus be ascribed either to POM release or to new composite properties arising from combination of TMC with $\{CoW_{11}TiO_{40}\}$. A steady uptake of FITC-labeled TMC/$\{CoW_{11}TiO_{40}\}$ nanocomposites over 24 h was observed for all concentrations with maximum overall uptake values around 15% (Fig. S8).

3.7. Drug release from TMC/$\{CoW_{11}TiO_{40}\}$ composites

The biodegradation properties of a given polymer matrix are decisive for its drug delivery applications: while M_v of the polymers should be in the appropriate range for renal clearance, degradation of the polymer is crucial for the release of the encapsulated drug. Chitosan and its derivatives are degraded through the hydrolyzation of glycosidic bonds by specific enzymes, such as lysozyme, chitosanase and β-glucosidase (Kean & Thanou, 2010; Zhang & Neau, 2001). The release of $\{CoW_{11}TiO_{40}\}$ from TMC/$\{CoW_{11}TiO_{40}\}$ nanocomposites was studied with dialysis methods. TMC/$\{CoW_{11}TiO_{40}\}$ was incubated with β-glucosidase and the cobalt content of aliquots of the release media was monitored with AAS after predetermined time intervals (Fig. 8) at pH 6, i.e. within the reported stability range for $\{CoW_{11}TiO_{40}\}$ (Wang et al., 2003; Yang et al., 2004).

Ca. 10% of $\{CoW_{11}TiO_{40}\}$ were released within the initial 3 h, followed by a slow but steady release over 24 h (Fig. 8). The onset of POM release is faster than that of $\{CoW_{11}TiO_{40}\}$–liposome complexes which slows down only after 14 h (Yang et al., 2004). $\{CoW_{11}TiO_{40}\}$–starch complexes, however, undergo decomposition within several hours (Wang et al., 2003).

3.8. In vitro cytotoxicity studies with TMC/$\{CoW_{11}TiO_{40}\}$ composites

Previous studies identified TMC with a degree of quaternization around 20% as non-toxic and biocompatible which renders it a convenient drug carrier (Kean & Thanou, 2010; Verheul et al., 2008). Cytotoxicity of TMC/$\{CoW_{11}TiO_{40}\}$ composites was investigated with MTT assays and compared to pristine $\{CoW_{11}TiO_{40}\}$ and TMC references. HeLa cells were incubated for 1, 2, 5 and 24 h with different concentrations (50, 25 and 12.5 μg) of the

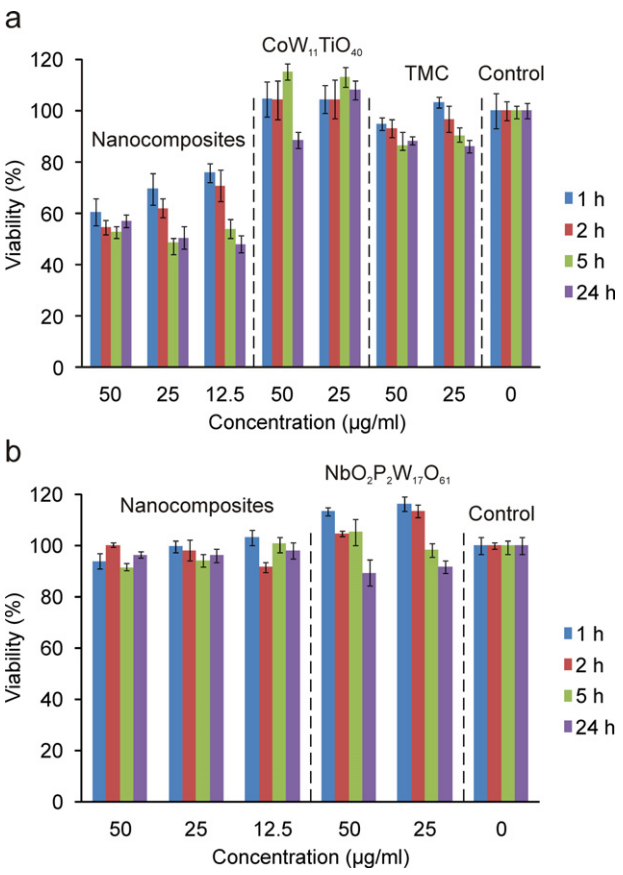

Fig. 9. (a) MTT assay of TMC/$\{CoW_{11}TiO_{40}\}$ composites, pristine $\{CoW_{11}TiO_{40}\}$ and pristine TMC for different concentrations (TMC/POM ratio = 1:0.1); (b) MTT assay of TMC/$\{NbO_2P_2W_{17}O_{61}\}$ composites and pristine $\{NbO_2P_2W_{17}O_{61}\}$ for different concentrations (TMC/POM ratio = 1:0.1).

compounds (Fig. 9). $\{CoW_{11}TiO_{40}\}$ alone does not affect the viability of HeLa cells, and this result differs clearly from previous observations on the significant anticancer activity of $\{CoW_{11}TiO_{40}\}$ under related experimental conditions (Wang et al., 2003; Yang et al., 2004). Pristine TMC lowers the cell viability only slightly after 24 h with no significant overall changes. TMC/$\{CoW_{11}TiO_{40}\}$ nanocomposites, however, significantly reduce HeLa cell viability after short treatment (1 h), and only 50% of the HeLa cells survive 5 h of exposition (Fig. 9). Longer incubation times did not lead to further changes in the cell viability. Reference experiments with $\{NbO_2P_2W_{17}O_{61}\}$ as an antiviral POM with no reported anticancer activity clearly demonstrate the full biocompatibility of both pristine $\{NbO_2P_2W_{17}O_{61}\}$ and TMC/$\{NbO_2P_2W_{17}O_{61}\}$ composites (Fig. 9b), thereby emphasizing the significant anticancer features of TMC/$\{CoW_{11}TiO_{40}\}$. Drug release from TMC/$\{CoW_{11}TiO_{40}\}$ nanocomposites showed a sharp release of 10% during the first 3 h and continued slowly and steadily afterwards (Fig. 8). Rapid uptake of TMC/$\{CoW_{11}TiO_{40}\}$ by HeLa cells at low composite concentrations was observed with final uptake values around 15%. Furthermore, micrographs of HeLa cells after incubation with TMC/$\{CoW_{11}TiO_{40}\}$ showed rounding effects that indicate a possible onset of cell death (Fig. 7). These observations in their entirety are in line with the reduction of HeLa cell viability to 50% after 5 h of treatment with TMC/$\{CoW_{11}TiO_{40}\}$ nanocomposites (Fig. 9). Composite-induced cell death proceeds more quickly in the initial hours of treatment, corresponding with faster POM release during the first 3–4 h (Fig. 8). The moderate absolute anticancer activity of TMC/$\{CoW_{11}TiO_{40}\}$ furthermore corresponds to slow overall POM release of ca. 20% over 24 h (Fig. 8).

Surprisingly, the reported anticancer activity of pristine $\{CoW_{11}TiO_{40}\}$ (Wang et al., 2003; Yang et al., 2004) could not be confirmed under comparable experimental conditions. However, this points to an enhanced antitumoral effect of the POM through encapsulation into the TMC drug carrier matrix. Note that a higher solution stability at pH 7.4 for TMC/$\{CoW_{11}TiO_{40}\}$ composites was observed than for pristine $\{CoW_{11}TiO_{40}\}$ (Fig. 2), which might contribute to the superior anticancer activity of the nanocomposites in comparison with the pristine POM. As mentioned above, uptake experiments in the presence of CP point to a different uptake pathway of POM–TMC composites in comparison with pristine TMC.

4. Conclusion

The present study demonstrates that both TMC and CMC are suitable drug carriers to encapsulate intact bio-active POMs. The different charges of the biopolymeric matrices significantly influence the properties of the resulting POM–CMC and POM–TMC nanocomposites. POM–CMC composites display negative zeta potentials and larger particle sizes than the positively charged POM–TMC composites. CMC favors the formation of spherical morphologies while TMC induces irregular particle shapes. Charge variations and morphological differences between CMC- and TMC-based nanoparticles lead to their different cellular uptake by HeLa cells. Whereas POM–TMC composites enter HeLa cells already at very low concentrations, 20-fold higher POM–CMC concentrations are required for a comparable extent of cellular uptake, probably due to the charge and morphology differences of both composite types. The favorable uptake properties of TMC matrices could thus be transferred upon new hybrid nanocomposites. Inhibition of the clathrin mediated pathway by chlorpromazine did not exert any negative effects on POM–CMC or POM–TMC composite uptake, while pristine CMC and TMC uptake, respectively, were hindered. Pre-incubation of HeLa cells with chlorpromazine, however, even promotes POM–TMC uptake, thus pointing to an alternative size-dependent uptake pathway. All in all, we have demonstrated that chemical tuning of chitosan-derived biopolymeric drug carriers for POMs can be applied to tune both physico-chemical and bio-active properties of the resulting nanocomposites. The multiple functionalities of TMC as a stabilizer, cellular shuttle and charge-inverting carrier for bio-active POMs open up new perspectives for the safe delivery of encapsulated POMs and for the exploration of their unknown metabolic pathways on the way to new inorganic drugs.

Acknowledgments

This work was supported by the Swiss National Science Foundation (SNSF Professorship PP00P2_133483/1) and financial support from the University of Zurich is gratefully acknowledged. We thank the Center for Microscopy and Image Analysis, ZMB, University of Zurich, for support. We thank Tamara Huber for the AAS analysis. The human cell line HeLa derived from cervical cancer was kindly provided by Prof. Peter Sonderegger (Department of Biochemistry, University of Zurich).

Appendix A. Supplementary data

Supplementary data associated with this article can be found, in the online version, at http://dx.doi.org/10.1016/j.carbpol.2012.08.009.

References

Alizadeh, M. H., Harmalker, S. P., Jeannin, Y., Martinfrere, J., & Pope, M. T. (1985). A heteropolyanion with fivefold molecular symmetry that contains a nonlabile encapsulated sodium ion. The structure and chemistry of $[NaP_5W_{30}O_{110}]^{14-}$. *Journal of the American Chemical Society*, *107*, 2662–2669.

Andrade, F., Goycoolea, F., Chiapetta, D. A., das Neves, J., Sosnik, A., & Sarmento, B. (2011). Chitosan-grafted copolymers and chitosan–ligand conjugates as matrices for pulmonary drug delivery. *International Journal of Carbohydrate Chemistry*, 1–14.

Borras-Almenar, J. J., Coronado, E., Müller, A., & Pope, M. T. (Eds.). (2004). *Polyoxometalate molecular science*. Dordrecht, The Netherlands: Kluwer.

Chen, Y. G., & Liu, J. F. (1997). Heteropoly complexes containing titanium. 2. Synthesis and characterization of titanotungstocobaltates. *Synthesis and Reactivity in Inorganic and Metal-Organic Chemistry*, *27*, 239–249.

Chen, X. G., & Park, H. J. (2003). Chemical characteristics of O-carboxymethyl chitosans related to the preparation conditions. *Carbohydrate Polymers*, *53*, 355–359.

Delmas, T., Piraux, H., Couffin, A.-C., Texier, I., Vinet, F., Poulin, P., et al. (2011). How to prepare and stabilize very small nanoemulsions. *Langmuir*, *27*, 1683–1692.

Dickman, M. H., Gama, G. J., Kim, K.-C., & Pope, M. T. (1996). The structures of europium(III)- and uranium(IV) derivatives of $[P_5W_{30}O_{110}]^{15-}$: Evidence for cryptohydration. *Journal of Cluster Science*, *7*, 567–583.

Edlund, D. J., Saxton, R. J., Lyon, D. K., & Finke, R. G. (1988). Trisubstituted heteropolytungstates as soluble metal oxide analogues. 4. The synthesis and characterization of organic solvent-soluble $(Bu_4N)_{12}H_4P_4W_{30}Nb_6O_{123}$ and $(Bu_4N)_9P_2W_{15}Nb_3O_{62}$ and solution spectroscopic and other evidence for the supported organometallic derivatives $(Bu_4N)_7[(C_5Me_5)Rh{\cdot}P_2W_{15}Nb_3O_{62}]$ and $(Bu_4N)_7[(C_6H_6)Ru{\cdot}P_2W_{15}Nb_3O_{62}]$. *Organometallics*, *7*, 1692–1704.

Fluetsch, A., Schroeder, T., Gruetter, M. G., & Patzke, G. R. (2011). HIV-1 protease inhibition potential of functionalized polyoxometalates. *Bioorganic & Medicinal Chemistry Letters*, *21*, 1162–1166.

Gaspar, V. M., Sousa, F., Queiroz, J. A., & Correia, I. J. (2011). Formulation of chitosan-TPP-pDNA nanocapsules for gene therapy applications. *Nanotechnology*, *22*, 1–12.

Geisberger, G., Paulus, S., Carraro, M., Bonchio, M., & Patzke, G. R. (2011). Synthesis, characterisation and cytotoxicity of polyoxometalate/carboxymethyl chitosan nanocomposites. *Chemistry – A European Journal*, *17*, 4619–4625.

Geisberger, G., Paulus, S., Gyenge, E. B., Maake, C., & Patzke, G. R. (2011). Targeted delivery of polyoxometalate nanocomposites. *Small*, *7*, 2808–2814.

Ginsberg, A. P. (Ed.). (1990). *Inorganic syntheses* (pp. 85–96). John Wiley & Sons, Inc.

Guan, M., Zhou, Y., Zhu, Q.-L., Liu, Y., Bei, Y.-Y., Zhang, X.-N., et al. (2012). N-trimethyl chitosan nanoparticle-encapsulated lactosyl-norcantharidin liver cancer therapy with high targeting efficacy. *Nanomedicine: Nanotechnology, Biology and Medicine*, http://dx.doi.org/10.1016/j.nano.2012.01.009

Han, Y.-K., Zhang, Z.-J., Wang, Y.-L., Xia, N., Liu, B., Xiao, Y., et al. (2011). An intriguing morphology evolution of polyoxometalate-polystyrene hybrid amphiphiles from vesicles to tubular aggregates. *Macromolecular Chemistry and Physics*, *212*, 81–87.

Harush-Frenkel, O., Debotton, N., Benita, S., & Altschuler, Y. (2007). Targeting of nanoparticles to the clathrin-mediated endocytic pathway. *Biochemical and Biophysical Research Communication*, *353*, 26–32.

Hasenknopf, B. (2005). Polyoxometalates: Introduction to a class of inorganic compounds and their biomedical applications. *Frontiers in Bioscience-Landmark*, *10*, 275–287.

Hill, C. L. (Ed.). (1998). *Chemical Reviews*, *98*, 1–389 (special issue on polyoxometalates)

Huang, M., Fong, C. W., Khor, E., & Lim, L. Y. (2005). Transfection efficiency of chitosan vectors: Effect of polymer molecular weight and degree of deacetylation. *Journal of Controlled Release*, *106*, 391–406.

Hungerford, G., Suhling, K., & Green, M. (2008). Luminescence enhancement of a europium containing polyoxometalate on interaction with bovine serum albumin. *Photochemical & Photobiological Sciences*, *7*, 734–737.

Inoue, M., Suzuki, T., Fujita, Y., Oda, M., Matsumoto, N., & Yamase, T. (2006). Enhancement of antibacterial activity of β-lactam antibiotics by $[P_2W_{18}O_{62}]^{6-}$, $[SiMo_{12}O_{40}]^{4-}$ and $[PTi_2W_{10}O_{40}]^{7-}$ against methicillin-resistant and vancomycin-resistant *Staphylococcus aureus*. *Journal of Inorganic Biochemistry*, *100*, 1225–1233.

Janes, K. A., Fresneau, M. P., Marazuela, A., Fabra, A., & Alonso, M. J. (2001). Chitosan nanoparticles as delivery systems for doxorubicin. *Journal of Controlled Release*, *73*, 255–267.

Jeong, Y.-I., Jin, S.-G., Kim, I.-Y., Pei, J., Wen, M., Jung, T.-Y., et al. (2010). Doxorubicin-incorporated nanoparticles composed of poly(ethylene glycol)-grafted carboxymethyl chitosan and antitumor activity against glioma cells in vitro. *Colloids and Surfaces B: Biointerfaces*, *79*, 149–155.

Jia, Z., Shen, D., & Xu, W. (2001). Synthesis and antibacterial activities of quaternary ammonium salt of chitosan. *Carbohydrate Research*, *333*, 1.

Judd, D. A., Nettles, J. H., Nevins, N., Snyder, J. P., Liotta, D. C., Tang, J., et al. (2001). Polyoxometalate HIV-1 protease inhibitors. A new mode of protease inhibition. *Journal of the American Chemical Society*, *123*, 886–897.

Kean, T., & Thanou, M. (2010). Biodegradation, biodistribution and toxicity of chitosan. *Advanced Drug Delivery Reviews*, *62*, 3–11.

Khor, E. (2001). *Chitin: Fulfilling a biomaterials promise*. Oxford: Elsevier Science., pp. 1–136.

Kraus, W., Stephan, H., Rollich, A., Matejka, Z., & Reck, G. (2005). $K_6H_2[TiW_{11}CoO_{40}]{\cdot}13H_2O$, with a monotitanoundecatungstocobaltate(II) anion. *Acta Crystallographica, Section E: Structure Report Online*, *61*, I35–I37.

Liang, Y., Sun, Y., Duan, Y., & Cheng, Y. (2012). Synthesis and characterization of PEG-graft-quaternized chitosan and cationic polymeric liposomes for drug delivery. *Journal of Applied Polymer Science*, *125*, 1302–1309.

Liu, X.-P., Zhou, S.-T., Li, X.-Y., Chen, X.-C., Zhao, X., Qian, Z.-Y., et al. (2010). Anti-tumor activity of N-trimethyl chitosan-encapsulated camptothecin in a mouse melanoma model. *Journal of Experimental & Clinical Cancer Research*, *29*, 76–84.

Mailaender, V., & Landfester, K. (2009). Interaction of nanoparticles with cells. *Biomacromolecules*, *10*, 2379–2400.

Meissner, T., Bergmann, R., Oswald, J., Rode, K., Stephan, H., Richter, W., et al. (2006). Chitosan-encapsulated Keggin anion $[Ti_2W_{10}PO_{40}]^{7-}$. Synthesis, characterization and cellular uptake studies. *Transition Metal Chemistry*, *31*, 603–610.

Menon, D., Thankam Thomas, R., Narayanan, S., Maya, S., Jayakumar, R., Hussain, F., et al. (2011). A novel chitosan/polyoxometalate nano-complex for anti-cancer applications. *Carbohydrate Polymers*, *84*, 887–893.

Mi, F.-L., Wu, Y.-Y., Lin, Y.-H., Sonaje, K., Ho, Y.-C., Chen, C.-T., et al. (2008). Oral delivery of peptode drugs using nanoparticles self-assembled by poly(γ-glutamic acid) and a chitosan derivative functionalized by trimethylation. *Bioconjugate Chemistry*, *19*, 1248–1255.

Miras, H. N., Cooper, G. J. T., Long, D.-L., Boegge, H., Mueller, A., Streb, C., et al. (2010). Unveiling the transient template in the self-assembly of a molecular oxide nanowheel. *Science*, *327*, 72–74.

Moskovitz, B. L., & The HPA-23 Cooperative Study Group. (1988). Clinical trial of tolerance of HPA-23 in patients with acquired immune deficiency syndrome. *Antimicrobial Agents and Chemotherapy*, *32*, 1300–1303.

Mourya, V. K., & Inamdar, N. N. (2009). Trimethyl chitosan and its application in drug delivery. *Journal of Material Science: Materials in Medicine*, *20*, 1057–1079.

Mourya, V. K., Inamdar, N. N., & Tiwari, A. (2010). Carboxymethyl chitosan and its applications. *Advanced Material Letters*, *1*, 11–33.

Mueller, C. E., Iqbal, J., Baqi, Y., Zimmermann, H., Roellich, A., & Stephan, H. (2006). Polyoxometalates – a new class of potent ecto-nucleoside triphosphate diphosphohydrolase (NTPDase) inhibitors. *Bioorganic & Medicinal Chemistry Letters*, *16*, 5943–5947.

Nam, H. Y., Kwon, S. M., Chung, H., Lee, S.-Y., Kwon, S.-H., Jeon, H., et al. (2009). Cellular uptake mechanism and intracellular fate of hydrophobically modified glycol chitosan nanoparticles. *Journal of Controlled Release*, *135*, 259–267.

Ni, L., Greenspan, P., Gutman, R., Kelloes, C., Farmer, M. A., & Boudinot, F. D. (1996). Cellular localization of antiviral polyoxometalates in J774 macrophages. *Antiviral Research*, *32*, 141–148.

Pahwa, P., Saini, N., Kumar, V., & Kohli, K. (2012). Chitosan-based gastroretentive floating drug delivery technology: An updated review. *Expert Opinions in Drug Delivery*, *9*, 525–539.

Park, S., Lee, S. J., Chung, H., Her, S., Kim, K., Choi, Y., et al. (2010). Cellular uptake pathway and drug release characteristics of drug-encapsulated glycol chitosan nanoparticles in live cells. *Microscopy Research and Technique*, *73*, 857–865.

Peng, S.-F., Tseng, M. T., Ho, Y.-C., Wei, M.-C., Liao, Z.-X., & Sung, H.-W. (2011). Mechanisms of cellular uptake and intracellular trafficking with chitosan/DNA/poly(gamma-glutamic acid) complexes as a gene delivery vector. *Biomaterials*, *32*, 239–248.

Polnok, A., Verhoef, J. C., Borchard, G., Sarisuta, N., & Junginger, H. E. (2004). In vitro evaluation of intestinal absorption of desmopressin using drug-delivery systems based on superporous hydrogels. *International Journal of Pharmaceutics*, *269*, 303–310.

Pope, M. T., & Mueller, A. (Eds.). (1994). *Polyoxometalates: From platonic solids to antiretroviral activity*. Dordrecht: Kluwer.

Prudent, R., Moucadel, V., Laudet, B., Barette, C., Lafanechere, L., Hasenknopf, B., et al. (2008). Identification of polyoxometalates as nanomolar noncompetitive inhibitors of protein kinase CK2. *Chemistry & Biology*, *15*, 683–692.

Rhule, J. T., Hill, C. L., & Judd, D. A. (1998). Polyoxometalates in medicine. *Chemical Reviews*, *98*, 327–357.

Shi, X. W., Du, Y. M., Yang, J. H., Zhang, B. Z., & Sun, L. P. (2006). Effect of degree of substitution and molecular weight of carboxymethyl chitosan nanoparticles on doxorubicin delivery. *Journal of Applied Polymer Science*, *100*, 4689–4696.

Shigeta, S., Mori, S., Watanabe, J., Soeda, S., Takahashi, K., & Yamase, T. (1997). Synergistic anti-influenza virus A (H1N1) activities of PM-523 (polyoxometalate) and ribavirin in vitro and in vivo. *Antimicrobial Agents and Chemotherapy*, *41*, 1423–1427.

Shigeta, S., Mori, S., Yamase, T., Yamamoto, N., & Yamamoto, N. (2006). Anti-RNA virus activity of polyoxometalates. *Biomedicine & Pharmacotherapy*, *60*, 211–219.

Slütter, B., & Jiskoot, W. (2010). Dual role of CpG as immune modulator and physical crosslinker in ovoalbumin loaded N-trimethyl chitosan (TMC) nanoparticles for nasal vaccination. *Journal of Controlled Release*, *148*, 117–121.

Sonia, T. A., & Sharma, C. P. (2011). Chitosan and its derivatives for drug delivery perspective. *Advances in Polymer Science*, *243*, 23–54.

van der Lubben, I. M., Verhoef, J. C., Borchard, G., & Junginger, H. E. (2001). Chitosan and its derivatives in mucosal drug and vaccine delivery. *European Journal of Pharmaceutical Sciences*, *14*, 201–207.

van der Merwe, S. M., Verhoef, J. C., Verheijden, J. H. M., Kotzé, A. F., & Junginger, H. E. (2004). Trimethylated chitosan as polymeric absorption enhancer for improved peroral delivery of peptide drugs. *European Journal of Pharmaceutics and Biopharmaceutics*, *58*, 225–235.

Verheul, R. J., Amidi, M., van der Wal, S., van Riet, E., Jiskoot, W., & Hennink, W. E. (2008). Synthesis, characterization and in vitro biological properties of O-methyl free N,N,N-trimethylated chitosan. *Biomaterials*, *29*, 3642–3649.

Verma, A., & Stellacci, F. (2010). Effect of surface properties on nanoparticle–cell interactions. *Small*, *6*, 12–21.

Wan, A. J., Sun, Y., Li, W.-T., & Li, H.-L. (2008). Transmission electron microscopy and electron diffraction study of BSA-loaded quaternized chitosan nanoparticles. *Journal of Biomedical Materials Research. Part B: Applied Biomaterials*, *86B*, 197–207.

Wang, X. H., Liu, J. F., & Pope, M. T. (2003). New polyoxometalate/starch nanomaterial: Synthesis, characterization and antitumoral activity. *Dalton Transactions*, *5*, 957–960.

Wang, X. H., Li, F., Liu, S. X., & Pope, M. T. (2005). New liposome-encapsulated-polyoxometalates: Synthesis and antitumoral activity. *Journal of Inorganic Biochemistry*, *99*, 452–457.

Wang, Z. H., Wang, Z. Y., Sun, C. S., Wang, C. Y., Jiang, T. Y., & Wang, S. L. (2010). Trimethylated chitosan-conjugated PLGA nanoparticles for the delivery of drugs to the brain. *Biomaterials*, *31*, 908–915.

Yang, Y., He, J. H., Wang, X. H., Li, B., & Liu, J. F. (2004). Preparation, characterization and in vitro antitumoral activity of a nanosize liposome complex encapsulated polyoxotungstate $K_6H_2[CoW_{11}TiO_{40}]$. *Transition Metal Chemistry*, *29*, 96–99.

Zhai, F., Li, D., Zhang, C., Wang, X., & Li, R. (2008). Synthesis and characterization of polyoxometalates loaded starch nanocomplex and its antitumoral activity. *European Journal of Medicinal Chemistry*, *43*, 1911–1917.

Zhang, H., & Neau, S. H. (2001). In vitro degradation of chitosan by a commercial enzyme preparation: Effect of molecular weight and degree of deacetylation. *Biomaterials*, *22*, 1653–1658.

Zhang, G., Keita, B., Craescu, C. T., Miron, S., de Oliveira, P., & Nadjo, L. (2007). Polyoxometalate binding to human serum albumin: A thermodynamic and spectroscopic approach. *Journal of Physical Chemistry B*, *111*, 11253–11259.